Oscillatory discharge behavior in Hall thrusters: relationships between the discharge current, electric field and microturbulence

IEPC-2017-443

Presented at the 35th International Electric Propulsion Conference
Georgia Institute of Technology – Atlanta, Georgia – USA
October 8–12, 2017

Sedina Tsikata*
CNRS, ICARE, EP Team, 1C ave. de la Recherche Scientifique, 45071 Orléans, France

Anne Héron†
CNRS, CPHT, Ecole Polytechnique, Route de Saclay, 91128 Palaiseau, France

Cyrille Honoré‡
CNRS, LPP, Ecole Polytechnique, Route de Saclay, 91128 Palaiseau, France

The dynamic nature of the Hall thruster discharge poses a challenge for a comprehensive physical understanding of the device. In this work, we examine the oscillatory behavior of the Hall thruster discharge issue via analysis of collective Thomson scattering (CTS) measurements of microturbulence and two-dimensional axial-azimuthal particle-in-cell simulations.

In CTS experiments, clear correlations between the time-varying discharge current and small-scale electron density fluctuations (associated with the electron cyclotron drift instability (ECDI)) are found across a wide voltage range. In simulations, the temporal evolution of the discharge current, the accelerating electric field, and the ECDI amplitude are compared in different operating regimes. In regimes with large discharge current oscillations, fluctuations in the discharge current are well-correlated with fluctuations in the ECDI field. In addition, such regimes show axial localizations of both the accelerating electric field and the ECDI field which vary in time. Results from both simulations and experiments support the notion of a time-varying, regime-dependent contribution of the ECDI to electron transport.

*Researcher, CNRS, ICARE, sedina.tsikata@cnrs-orleans.fr
†Researcher, CNRS, CPHT, Ecole Polytechnique, Université Paris Saclay, anne.heron@polytechnique.edu
‡Research Engineer, LPP, CNRS, Ecole Polytechnique, UPMC Univ Paris 06, Univ. Paris-Sud, Observatoire de Paris, Université Paris-Saclay, Sorbonne Universités, PSL Research University, cyrille.honore@polytechnique.edu

I. Introduction

THE importance of anomalous electron transport in determining the operation of a range of plasma sources is widely acknowledged. In Hall thrusters, anomalous electron transport plays a significant role at the exit plane region of the thruster, where the electron mobility exceeds the classical mobility by a few orders of magnitude. Recent research efforts in the community have sought to understand possible mechanisms responsible for this, and different plasma instabilities have often been cited as potential contributors.

The electron cyclotron drift instability (ECDI) is an instability whose role in electron transport has been studied in important papers by authors such as Gary and Sanderson,[8] Forslund et al.,[7] and many others. 2D particle-in-cell (PIC) simulations performed by Adam, Héron and Laval[1] first showed the presence of the ECDI for a standard Hall thruster plasma. This work was the impetus for experimental (coherent/collective Thomson scattering (CTS)) and theoretical studies a few years later confirming the presence of the instability and providing detailed characterizations of its features.[3,14,16] Additional simulations designed to study radial effects have provided evidence for the complexity of the instability's role in transport. This role is a dual one, important not only due to the mode's direct interaction with electrons, but also due to its role in increasing electron emission from walls via radial heating.[9] Other particle-in-cell studies on the instability have emerged in recent years.[4,10]

While numerical studies support a role for the ECDI in transport, it is worth mentioning that other instabilities at longer length scales may also play a role in transport, as suggested by other studies.[6,11,12] Understanding the relationship between different scales and the role played by different instabilities across operating regimes is an interesting challenge in the field today. Observations made in the context of other sources (planar magnetrons) provide evidence for the persistence of ECDI-scale electron density fluctuations within large-scale structures like spokes, which may ultimately drive transport in such zones.[17]

One interesting aspect to consider is whether the influence of such instabilities can be clearly linked to global features of the discharge: discharge current, performance, regime transitions and so on. For instance, the appearance of a beam-plasma instability[9,13] may be linked to the jumps in the electron current or regime changes, as speculated in Refs. 13 and 9. Are such influences detectable through measurements?

This work examines this question for the ECDI, drawing on experimental measurements and information obtained from numerical simulations.

II. Methodology

A. The role of the ECDI in transport: evidence to date

So far, the most direct evidence for the role of ECDI in electron transport has been gained from self-consistent PIC simulations,[1] which show unambiguously the following:

(i) at given instants during the simulation run time, the mean electron velocity becomes sharply negative (directed towards the anode). These instants correspond to the same times at which different modes of the instability appear (with different modes represented by different integer values of n, where $n = k_y V_d/\omega_{ce}$, with k_y the mode azimuthal wave number, V_d the electron azimuthal drift velocity, and ω_{ce} the electron cyclotron frequency. These different values of n correspond to the different cyclotron resonances at which the mode is excited). The appearance of the negative axial electron velocity at the same time as the appearance of different ECDI modes was shown in the 2006 thesis of A. Ducrocq.[5]

(ii) the anomalous electron current in PIC simulations can be largely attributed to the ECDI alone, in the exit plane region, with no other mechanism required to find the correct levels of overall current. The evolution of the instability and the electron current are strongly linked: when the non-linear growth phase of the instability is reached and the mode saturates, accompanied by the flattening of the electron energy distribution functions, the electron current also saturates.

CTS experiments have been successful in measuring electron density fluctuations on the same length scales as those of the ECDI. These measurements find the mode frequencies and wavenumbers expected from the simulations and from linear kinetic theory analysis. While in simulations, the level of electron current can be tracked directly against the mode growth, linking the level of electron current directly to the experimentally-measured density fluctuations is a challenge, since:

(i) precise knowledge of the fraction of the overall discharge current which constitutes the electron current is required. Unfortunately, available diagnostic methods (such as Faraday cups to determine the ion current) lack sufficient precision to allow the electron current fraction to be accurately measured.

(ii) absolute form factor measurements obtained from CTS[16] correspond to the *saturated* density fluctuation level. This means that the evolution in the mode amplitude during the linear and non-linear growth phases cannot be tracked.

B. Time-resolved analysis

To overcome these limitations, it is necessary to focus on different analysis methods which preserve the time-varying character of the measured fluctuations.

In CTS measurements, the scattered power arriving at the detector is due to interference between two fields: the scattered ECDI field, and a frequency-shifted reference field known as the local oscillator (defined by a modulation frequency ω_m and phase ϕ_m). This mixing is used to set up a heterodyne detection scheme which facilitates detection of the plasma-scattered field.

The time-varying power arriving at the detector is converted into a time-varying electric current by the photovoltaic effect, and this current can directly be related to the plasma-scattered, complex signal (dependent on the set observation wavevector and time), known as $s(\vec{k}, t)$.

A series of demodulation steps, involving (a) multiplication by a reference signal of frequency ω_m, and (ii) filtering of the resulting high-frequency $2\omega_m$ terms allows the recovery of the complex scattered signal:

$$s(\vec{k}, t) \propto e^{i\phi_m}[x_f(t) - iy_f(t)] \quad (1)$$

In the practical application of the demodulation scheme, the individual $x_f(t)$ and $y_f(t)$ components are recovered on separate measurement channels and the complex $s(\vec{k}, t)$ can be then reconstructed.

The $x_f(t)$ and $y_f(t)$ components are time-varying signals recorded over the acquisition duration, which is typically as long as 65 ms in our experiments. As explained in earlier works, the long acquisition time (compared to the period of the MHz-scale instability) provides sufficient statistics to perform signal averaging to extract the weak plasma-scattered signal from the noise background.

In form factor calculations, Fourier transforms are performed on short segments of the signal and these spectra are then averaged. The spectra are then normalized to remove electronics and photonic noise to give the dynamic form factor $S(k, \omega)$, which expresses the intensity of the electron density fluctuations for a given wavenumber over a frequency range. The form factor, $S(k)$, is an absolute measurement of the intensity of these density fluctuations and results from the integral of the dynamic form factor over the frequency range.

Rather than use these measurements, we can focus on the time variation of the absolute value of the signal $s(\vec{k}, t)$. This provides a qualitative measurement of the density fluctuation, which can then be correlated directly with the time-varying discharge current, which is acquired simultaneously with the same measurement system.

The analysis procedure for a typical signal acquisition is performed according to the following steps. The standard signal normalization procedures are first performed to determine the dynamic form factor, from which a Gaussian central peak frequency μ_f and peak width σ_f are defined.

The individual time-dependent components of the complex signal are separately filtered using a 10 MHz low-pass filter, in order to remove remaining high-frequency parasitic frequency components, and the absolute value of the signal is calculated ($\sqrt{x(t)^2 + y(t)^2}$).

The short time Fourier transform of this absolute signal is shown in Fig. 1. This spectrogram plot has been determined using a window of 1000 points, 980 overlapping points, and short segments of 4096 points over which the Fourier transform is calculated. The sampling frequency is 100 MHz.

Figure 1 shows a plot of frequency, time and amplitude (amplitude defined as 10 $log_{10}(P)$, where P is the power spectral density) for an acquisition made at 120 V. This figure shows clearly the appearance of a signal peak, corresponding to the ECDI signal, at around 2 MHz, and additionally, a low-frequency oscillation in the amplitude of this MHz-scale mode, on the order of a few kHz. The significance of this low-frequency oscillation and the voltage regime considered is discussed in the next section.

In order to compare this oscillation to the discharge current, the power spectral densities are integrated over the frequency range $[-3\sigma_f; 3\sigma_f]$ around μ_f at every time step, for a given frequency integration step f_s. This produces a single time-varying series (which we shall call $\Sigma P(t)$), reflecting the integrated ECDI signal fluctuations. This data is correlated with the discharge current.

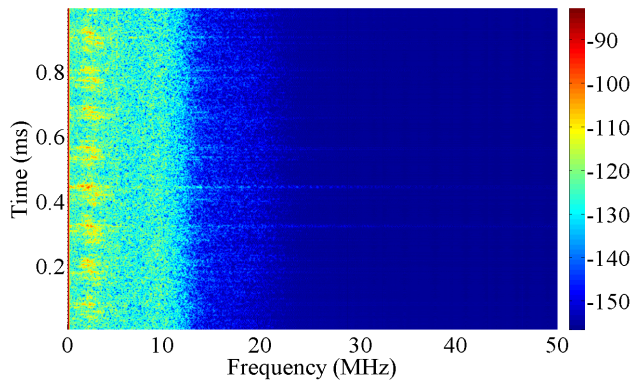

Figure 1. Spectrogram of the absolute time-varying signal from the CTS experiment (120 V) showing a low-frequency variation of the signal amplitude over time and the localization of the signal of interest around 2 MHz

For the correlation results discussed in this paper, the length of the signal series used is 1×10^6 points, acquired at a frequency of 100 MHz (corresponding to a total time duration of 10 ms). Note that Fig. 1 shows only a shortened duration (1 ms) for the sake of clarity. The time step at which each integrated spectral density is calculated corresponds to 2.2×10^{-7} s; this gives the time resolution. The discharge current sampling at 100 MHz is downscaled to match this time step before the correlation is calculated.

III. Correlations between ECDI fluctuations and discharge current

The maximum cross-correlation coefficients, identified by c, were determined between the scattered signal $\Sigma P(t)$ and the discharge current, which we shall identify by I_d.

Fig. 2(a) shows these coefficients determined over a range of discharge voltage values for the 1.5 kW PPS 1350-ML thruster,[15] operated at a 3.5 mg/s xenon flow rate and for a magnetic coil current of 4.5 A. Experiments were performed with the observation volume positioned 11 mm outside the thruster exit plane. The signals recorded in the scattering experiments were processed using the procedures outlined in the preceding section.

As Fig. 2(a) shows, the correlations between the scattered signal and the discharge current are significant and vary according to the particular voltage regime. For the purposes of discussion, the voltage regions have been divided into 3 regimes (shown using dashed vertical lines in Fig. 2(a)). Yet this division is not arbitrary; in fact, over the full range of voltages explored, the value of the correlation coefficient varies in a manner which is similar to the fluctuation in the discharge current. The accompanying discharge current fluctuations ($\sigma(Id)$) at each voltage are shown in Fig. 2(b). An increasing correlation between the ECDI signal and discharge current occurs with increasing discharge current fluctuations. Moderate correlations correspond to lower discharge current fluctuations.

These regimes can be distinguished further:

1. **Regime 1**: below 100 V, the discharge has not yet reached maximum ionization and the mean discharge current increases with voltage before saturating (not shown). In regime 1, the discharge current oscillates with frequencies of only a few kHz (and accompanying harmonics). Floating probes placed at the thruster exit plane reveal that these frequencies correspond to an axial oscillation of the ionization region.

2. **Regime 2**: in this intermediate regime, the familiar "breathing mode"[2] oscillations at frequencies of tens of kHz appear, associated with more moderate and less coherent discharge current fluctuations.

3. **Regime 3**: in this higher-voltage regime discharge current fluctuations increase before again decreasing. The breathing mode oscillations remain present throughout.

The total time-varying power spectral density of the scattered signal $\Sigma P(t)$ is superposed on the discharge current to visually illustrate the difference in regimes, and these results are shown in Fig. 3.

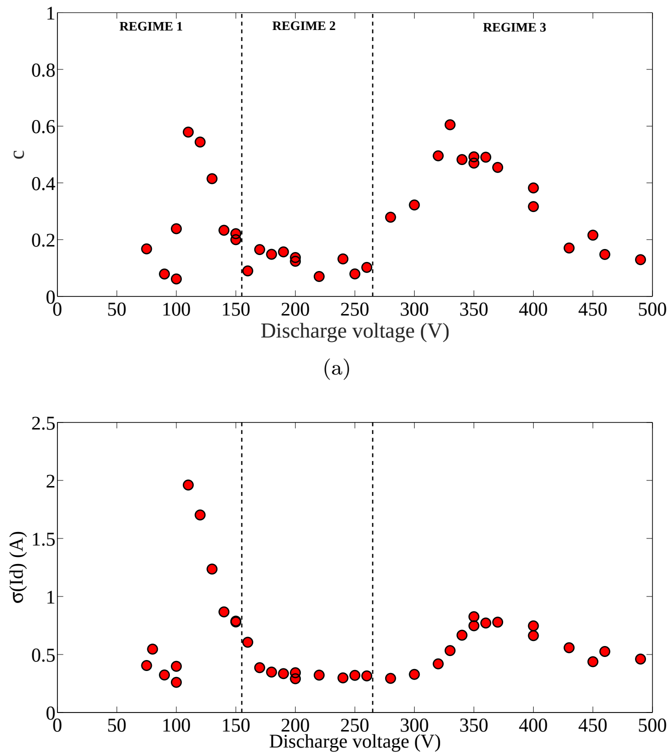

(a)

(b)

Figure 2. (a) Cross-correlation coefficients (c) determined between the scattered signal associated with the ECDI ($\Sigma P(t)$) and the simultaneously-recorded discharge current Id. The degree of correlation is significant across all voltage values. Vertical dashed lines are used to denote different regimes discussed in the text. (b) Level of discharge current fluctuations ($\sigma(Id)$) determined for points shown in Fig. 2(a).

Fig. 3 shows a reduced time series (up to 3 ms) for each operating regime in order to improve visibility. This figure presents examples from the three different discharge current oscillation regimes described, showing the oscillation of the ECDI signal. The presence of similar oscillations in both the discharge current and ECDI signal are easy to identify.

Returning now to the correlation coefficients presented in Fig. 2(a), it should be noted that these maximum correlation values correspond to specific time shifts (c_{lag}) between $\Sigma P(t)$ and Id. The values of these time shifts are now shown in Fig. 4.

In Fig. 4, positive time values correspond to cases for which the scattered signal *precedes* the discharge current; for negative time values, fluctuations appear in the recorded discharge current before they are seen in the scattered signal record. Fig. 4 shows the scattered signal preceding the discharge current for several voltages, with a time shift on the order of 10^{-5} s at lower voltages, and time shifts on the order of a few microseconds for higher voltages. What exactly is the significance of these time lags?

Possible interpretations

The positive sign of the time shift may suggest that we can visualize the action of the ECDI in the following way.

Experimental measurements (with CTS) are performed at 11 mm chiefly because the maximum density fluctuations have been observed close to, or at, this position for the typical thruster operating parameters. These density fluctuations are expected to be associated with the ECDI. The action of the ECDI, if the mode does contribute to the de-trapping of the electrons and anomalous electron current, may be visible in corresponding fluctuations first in the observation volume before fluctuations are registered in the discharge current (which is measured inside the channel, at the anode). This would account for the EDCI signal fluctuations preceding the discharge current fluctuations.

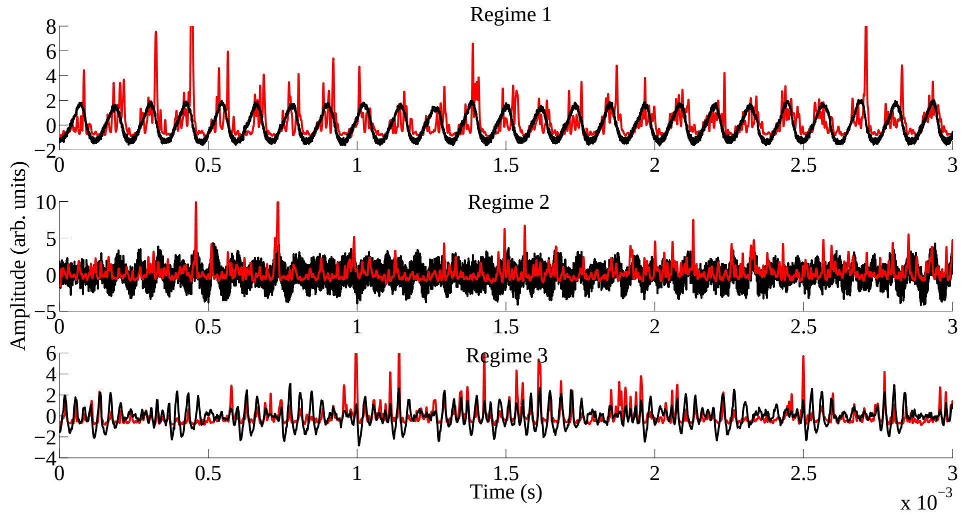

Figure 3. Superposed discharge current and ECDI signal integrated power spectral density for different regimes of discharge current oscillation: regime 1 (120 V), regime 2 (200 V) and regime 3 (350 V).

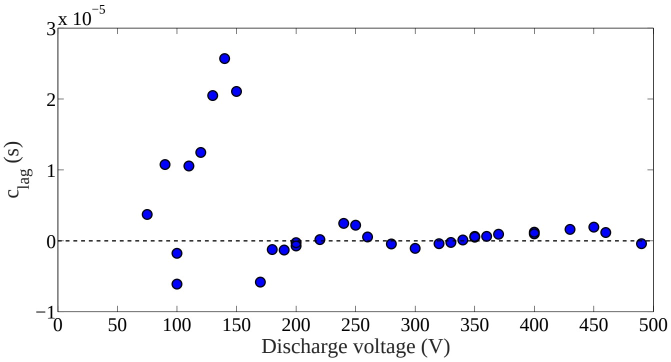

Figure 4. Correlation time lags corresponding to coefficients shown in Fig. 2(a)

We can also note that PIC simulations calculate an axial electron drift velocity associated with the appearance of the ECDI which is on the order of tens of km/s, according to the work of Ducrocq.[5] If we use this velocity to estimate a time of flight for electrons between the experimental observation volume position and the anode (where the discharge current is measured) we find a time of flight on the order of a few μs. This is compatible with the positive time lag determined in directly from experiments.

This is, of course, a simplistic interpretation of electron behavior resulting in anomalous current. As a first approximation it assumes that the fluctuations in electron current can be attributed to a simple axial drift; simulations of the electron current density reveal the formation of very complex electron current structures and even "recirculating" electrons. In addition, the existence of some negatively-signed correlation times does not match the simple explanation advanced. One possible reason for which fluctuations in the discharge current may precede fluctuations measured in the observation volume may be the action of large-scale oscillations of the plasma, or even the observation of electrons from the ionization region reaching the anode before convection outside the thruster. In any case, it will be important to devise specific experiments to test these ideas.

IV. Simulation analyses

The results described in the previous section show, from experiments, that the discharge current and density fluctuations associated with the ECDI are correlated. We now turn our attention to the information accessible in simulations: the accelerating electric field, ECDI field, and discharge current.

In fully-2D particle-in-cell axial-azimuthal simulations,[1] the accelerating electric field (which we shall identify by E_a) is self-consistently calculated, as are the associated ECDI field (E_f) and discharge current (Id). Analysis of the correlations between these different elements reveals interesting features, described in this section. Rather than be considered a direct comparison to the voltage regimes in the preceding sections, these simulation conditions should be considered as representative of "nominal" thruster operation (at 300 V) and high voltage thruster operation (at 800 V). The applied magnetic field has the same profile and intensity as that depicted in Ref. 1.

A. Correlations between the applied and ECDI fields

1. 300 V case

To depict the time-varying character of the ECDI and accelerating fields, the fields are summed in the azimuthal direction of the simulation and this integrated variation in intensity is shown as a function of the simulation time and the axial position.

Fig. 5 shows the accelerating and ECDI fields (in units of V/m) at 300 V using this analysis. The exit plane corresponds to the 0 cm axial position. The accelerating field is not static: its axial localization and amplitude vary with time. The field enters the channel at particular instants in the simulation, and these incursions into the channel are accompanied by increases in the accelerating field amplitude. The ECDI field shows variations closely related to the accelerating field. It also shows increases in amplitude coinciding with the instants when the accelerating field enters the channel.

In fact, these observations are similar to what we have seen with carbon velvet. Movement of the accelerating field into the channel, which accompanies the use of carbon velvet at the thruster exit plane, is expected to result in higher ECDI amplitudes.[15]

2. 800 V case

The correlations between the ECDI and accelerating fields are even more striking at higher voltages. This is illustrated by the 800 V case, shown in Fig 6, analyzed using the same technique as for Fig. 5.

Fig. 6(a) shows large-amplitude axial displacements of the accelerating electric field, compared to the 300 V case. Corresponding shifts in the ECDI field localization, along with increases in the ECDI field amplitude at the same times, are observable in Fig. 6(b).

These results are indication that there is no true "steady-state" behavior, and this has consequences for the expected electron transport driven by the ECDI, which will continually fluctuate. An initially high accelerating electric field will be at the origin of a high ECDI field amplitude. This will in turn increase the electron transport due to the ECDI, thus lowering the maximum accelerating electric field which can be achieved. This will then, in turn, depress the ECDI amplitude, lowering the electron transport, and allowing the electric field to increase again.

The time-varying behavior of the accelerating and ECDI fields appears to be reflected in the discharge current, as the next section shows.

B. Correlations between the ECDI field and discharge current

The simulations allow a direct comparison of the temporal variation of the accelerating field, ECDI field and the discharge current. This comparison is considered for both 300 and 800 V regimes.

At 11 mm from the exit plane (again chosen because this is the axial position identified in experiments as the location of the maximum ECDI density fluctuation in several cases), the time-varying values of the ECDI and accelerating fields are extracted (from Figs. 5 and 6) and normalized. These profiles are superposed on the normalized discharge current determined from the simulations. Results are shown in Fig. 7 for both voltages.

At 300 V, Fig. 7(a) shows correlated fluctuations in the accelerating field and ECDI signal, however, correlation with the discharge current is less evident. The 300 V regime in the simulations corresponds to a regime of moderate discharge current fluctuation (a standard deviation of 12% of the mean current). In experiments, regimes of moderate discharge current fluctuation coincide with lower correlations between the ECDI and the discharge current.

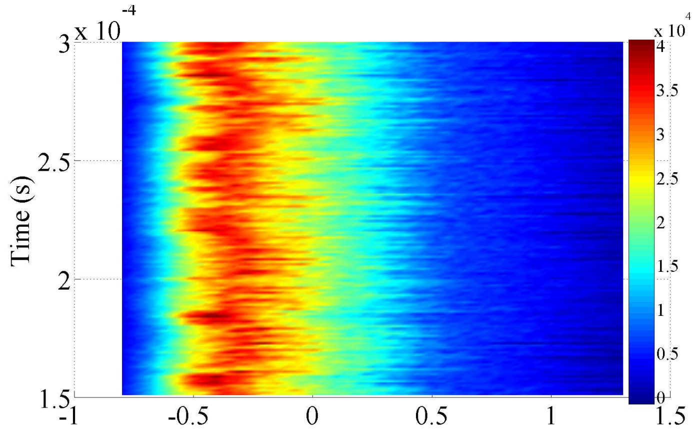

(a)

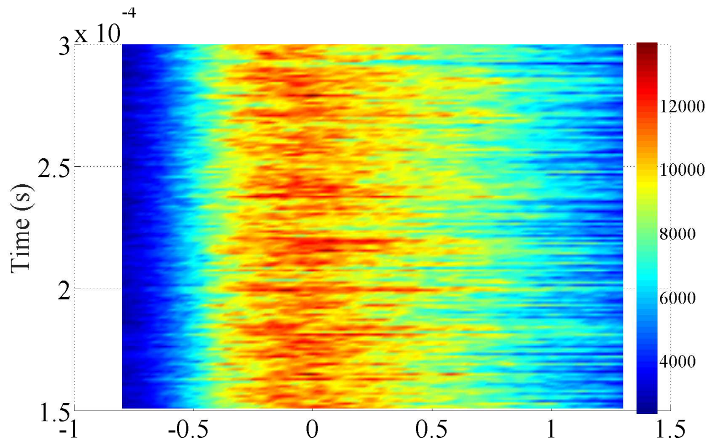

(b)

Figure 5. (a) Self-consistent accelerating field at 300 V (b) accompanying ECDI field at 300 V. These figures show the fields integrated over the simulation azimuthal direction (units of V/m).

At 800 V, Fig. 7(b) shows the following: (i) correlated fluctuations in the accelerating and ECDI fields, and (ii) strongly-correlated fluctuations in the ECDI field and the discharge current. We note that these simulations do not have the time resolution accessible (0.22 μs) in the experimental analyses presented earlier, which showed μs-scale time shifts between the ECDI fluctuations and the discharge current. In these simulations (with a time step of 1 μs) the ECDI and discharge current appear to be in phase. At 800 V, we note that discharge current fluctuations (standard deviation) are 40% of the discharge current. As in experiments, regimes characterized by large discharge current fluctuations show strong correlations between the ECDI and discharge current.

Fig. 8 shows the level of discharge current fluctuations (absolute current determined from the simulations, not normalized) for the 300 V and 800 V cases.

Although the ECDI has been identified in every voltage regime so far explored experimentally, on all thrusters so far investigated (ranging in power from 200 W to 5 kW), the relationship between this mode and its possible contribution to anomalous current is likely to depend on the operating regime. As illustrated above, with moderate discharge current oscillations, the correlations between the ECDI and discharge current are moderate. In regimes characterized by large discharge current fluctuations, the ECDI and discharge current are strongly correlated.

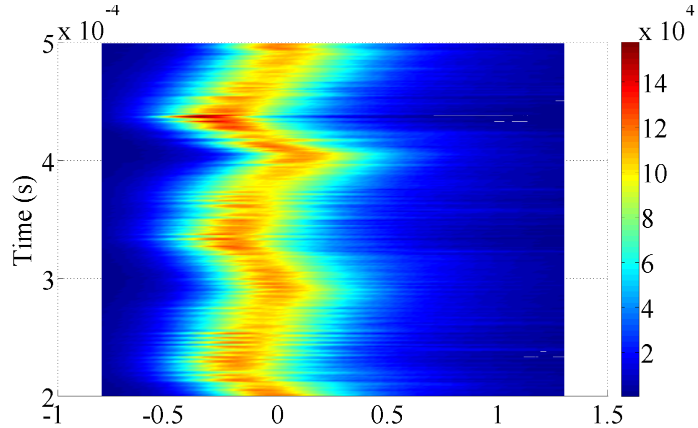

(a)

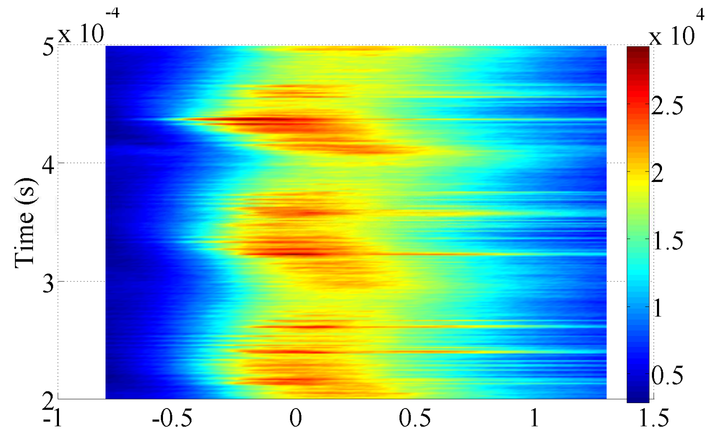

(b)

Figure 6. (a) Self-consistent accelerating field at 800 V (b) accompanying ECDI field at 800 V. These figures show the fields integrated over the simulation azimuthal direction (units of V/m).

V. Conclusions

In this paper, new approaches to understanding the role of the ECDI in electron transport are studied. In the first approach, the absolute signal measured in collective Thomson scattering experiments is analysed, in such a way as to preserve temporal information for direct comparison to the discharge current. This analysis reveals the presence of unambiguous correlations between the ECDI and discharge current fluctuations. In addition, the observation of ECDI fluctuations prior to fluctuations in the discharge current in many regimes may provide a direct and measurable clue as to the impact of the ECDI on the electron current, although further analysis will be required.

In the second approach, the information available from self-consistent axial-azimuthal PIC simulations - the time-varying accelerating electric field, ECDI field and discharge current amplitudes - is examined. Analysis of these features shows (i) a time-varying spatial localization of the accelerating and ECDI fields, (ii) the dependence of the ECDI fluctuations on this axial localization, and (iii) the strong correlations between the ECDI and discharge current in regimes of large discharge current fluctuation.

The experimental and numerical findings are compatible and the combination of these approaches may advance our current understanding of how the ECDI (as well as other modes, to be investigated in future studies) contribute to electron transport across different thruster operating regimes.

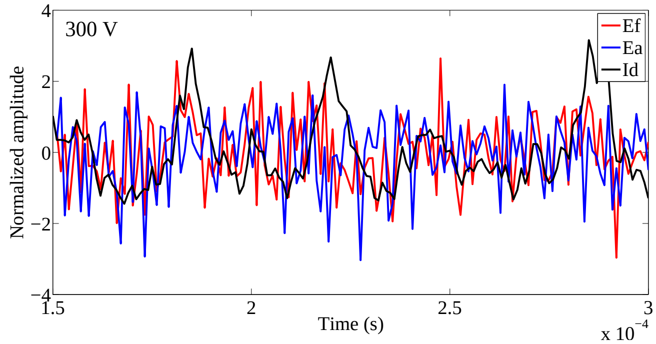

(a)

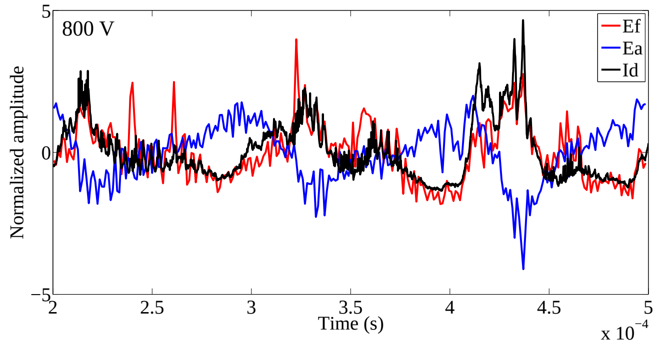

(b)

Figure 7. Superposed time-varying values of ECDI (Ef (red), accelerating field Ea (blue) and discharge current Id (black) determined in the axial-azimuthal simulations, for (a) 300 V and (b) 800 V.

References

[1] J-C. Adam, A. Héron, and G. Laval. *Phys. Plasmas*, 11:295, 2004.

[2] J-P. Boeuf and L. Garrigues. *J. Appl. Phys.*, 84:3541, 1998.

[3] J. Cavalier, N. Lemoine, G. Bonhomme, S. Tsikata, C. Honoré, and D. Grésillon. *Phys. Plasmas*, 20:082107, 2013.

[4] P. Coche and L. Garrigues. *Phys. Plasmas*, 21:023503, 2014.

[5] A. Ducrocq. *Rôle des instabilités électroniques de dérive dans le transport électronique du propulseur à effet Hall*. Ph.D. thesis, Ecole Polytechnique, Palaiseau, France, 2006.

[6] C. L. Ellison, Y. Raitses, and N. J. Fisch. *Phys. Plasmas*, 19:013503, 2012.

[7] D. W. Forslund, R. L. Morse, and C. W. Nielson. *Phys. Rev. Lett.*, 25:1266, 1970.

[8] S. Peter Gary and J. J. Sanderson. *J. Plasma Phys.*, 4:739, 1970.

[9] A. Héron and J-C. Adam. *Phys. Plasmas*, 20:082313, 2013.

[10] T. Lafleur, S. D. Baalrud, and P. Chabert. *Phys. Plasmas*, 23:053502, 2016.

[11] A. Lazurenko, L. Albarède, and A. Bouchoule. *Phys. Plasmas*, 13:083503, 2006.

[12] A. A. Litvak, Y. Raitses, and N. J. Fisch. *Phys. Plasmas*, 11:1701, 2004.

[13] D. Sydorenko, A. Smolyakov, I. Kaganovich, and Y. Raitses. *Phys. Plasmas*, 15:053506, 2008.

[14] S. Tsikata, C. Honoré, N. Lemoine, and D. M. Grésillon. *Phys. Plasmas*, 17:112110, 2010.

[15] S. Tsikata, A. Héron, and C. Honoré. *Phys. Plasmas*, 24:053519, 2017.

[16] S. Tsikata, N. Lemoine, V. Pisarev, and D. Grésillon. *Phys. Plasmas*, 16:033506, 2009.

[17] S. Tsikata and T. Minea. *Phys. Rev. Lett.*, 114:185001, 2015.

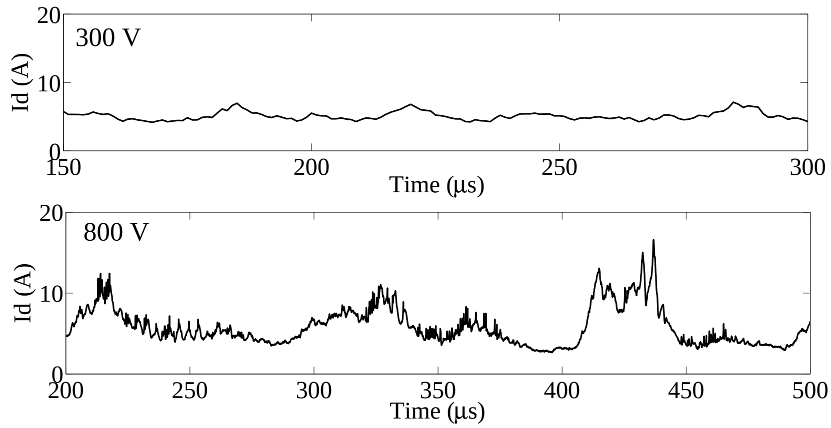

Figure 8. Variation of absolute discharge current with time for 300 and 800 V, in simulations